Uncertainty Quantification of Shear-induced Paraffin Droplet Pinch-off in Hybrid Rocket Motors

Georgios Georgalis*,¶
Tufts University, Medford, MA 02155, USA

Darsh Nathawani †,¶ and Matthew Knepley ‡ *University at Buffalo, The State University of New York, Buffalo, NY 14260, USA*

Abani Patra[§]
Tufts University, Medford, MA 02155, USA.

Hybrid rocket motors with paraffin-based fuels are of interest due to higher regression rates compared to other polymers. During paraffin combustion, a liquid layer forms on the fuel surface that, together with shearing forces from the oxidizer flow, results in the formation of instabilities at the fuel-oxidizer interface. These instabilities lead to the formation and entrainment of heterogeneous sized liquid droplets into the main flow and the combusting droplets result in higher motor output. The atomization process begins with droplet formation and ends with droplet pinch-off. The goal of this paper is to conduct an uncertainty quantification (UO) analysis of the pinch-off process characterized by a pinch-off volume (V_{po}) and time (t_{po}) . We study these quantities of interest (QoIs) in the context of a slab burner setup. We have developed a computationally expensive mathematical model that describes droplet formation under external forcing and trained an inexpensive Gaussian Process surrogate of the model to facilitate UQ. We use the pinch-off surrogate to forward propagate uncertainty of the model inputs to the QoIs and conduct two studies: one with gravity present and one without gravity effects. After forward-propagating the uncertainty of the inputs using the surrogate, we concluded that both QoIs have right-skewed distributions, corresponding to larger probability densities towards smaller pinch-off volumes and times. Specifically, for the pinch-off times, the resulting distributions reflect the effect of gravity acting against droplet formation, resulting in longer pinch-off times compared to the case where there is no gravity.

I. Nomenclature

G = Oxidizer mass flux

GaSP = Gaussian Stochastic Process LHS = Latin Hypercube Sampling

MC = Monte-Carlo

PDFs = Probability Distribution Function(s)

R = Port radius

 h_0 = Inlet radius of a forming droplet

 t_{no} = Pinch-off time

 u_0^l = Inlet velocity of a forming droplet UQ = Uncertainty Quantification

^{*}Data Scientist, Data Intensive Studies Center, 177 College Ave., Medford, MA 02155, USA. AIAA Member

[†]Graduate Research Assistant, Computational and Data-enabled Science and Engineering, University at Buffalo, The State University of New York, Buffalo, NY 14260, USA.

[‡]Assoc. Professor, Department of Computer Science and Engineering, University at Buffalo, The State University of New York, Buffalo, NY 14260, USA.

^{*}Director and Stern Family Professor, Data Intensive Studies Center and Department of Mathematics, Tufts University, Medford, MA 02155,

These authors contributed equally to this work.

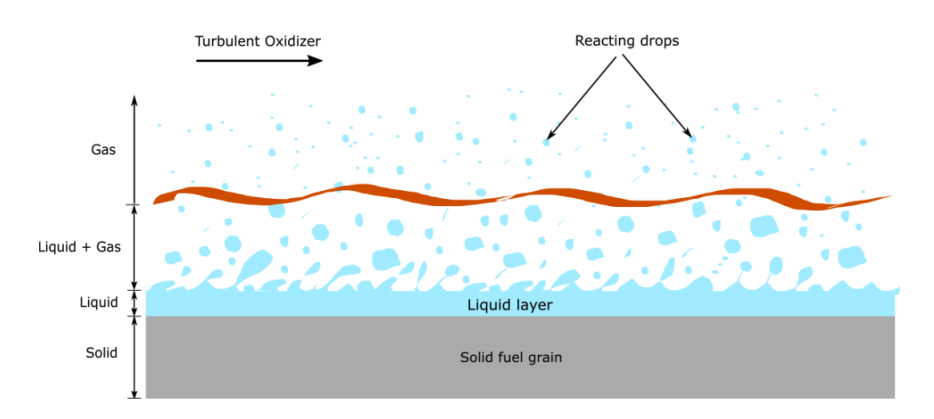


Fig. 1 Schematic of the solid fuel-liquid oxidizer interface and droplet atomization in a hybrid rocket slab burner setup [9].

 V_{po} = Pinch-off volume

 γ^l = Surface tension of liquid-gas interface

 $\mu^g = \text{Oxidizer dynamic viscosity}$ $v^g = \text{Oxidizer kinematic viscosity}$

 v^{l} = Liquid fuel kinematic viscosity μ^{l} = Liquid fuel dynamic viscosity

 $\rho^g = \text{Oxidizer density}$ $\rho^l = \text{Liquid fuel density}$ $p^g = \text{Combustion gas pressure}$

II. Introduction

Hybrid rocket motors are composed of the fuel and oxidizer in two different states, e.g., the fuel is solid and the oxidizer is a gas/liquid. Operation of hybrid rockets offers advantages as they can provide high energy density compared to solid bi-propellant systems, but with operational flexibility of liquid-only systems (e.g., shutoff, restart, less complicated piping) [1]. In terms of solid fuels in hybrid systems, it has been experimentally shown that paraffin-based fuels have higher regression rates compared to polymers [2]. The higher regression rates result from a different combustion mechanism of higher alkane solid fuels like paraffin, namely, the formation of a liquid layer on the surface which together with the formation of instabilities in the fuel-oxidizer interface [3] leads to entrainment of liquid droplets into the main flow [4]. The combusting droplets result in higher motor output performance. The regression of the fuel occurs both due to evaporation and atomization [4]. Here we focus on the droplet formation and entrainment and the uncertainty associated with the droplet formation process. The two main quantities of interest (QoIs) in the droplet pinch-off process are the pinch-off droplet volume (i.e., how large is the droplet) and the pinch-off time (i.e., how long it takes for the droplet to pinch-off), and both control fuel availability and thereby combustion. Precise modeling of droplet pinch-off is very challenging, but has been accomplished under certain assumptions (e.g., see [5] for a formulation on gravity-driven droplets assuming constant shear force, [6] for a 1D formulation that can simulate up to the first droplet, [7] for an axisymmetric non-linear atomization model, and [8] for a review). A schematic of the phenomena described is shown in Fig. 1.

The goal of this paper is to quantify the uncertainty associated with droplet pinch-off and its quantities of interest (QoIs): the pinch-off volume (V_{po}) and time (t_{po}) . In recent work [5, 9] have developed a first principles mathematical model and numerical solution methods that describe droplet formation under external forcing. The model simulates the formation and pinch-off of a droplet from the liquid paraffin layer, under shearing effects of the fast moving gaseous oxidizer. Understanding the uncertainty of droplet-pinch off will allow us to better account for the inherent variations in the droplet sizes that are produced during combustion of paraffin-based fuels, and therefore characterize performance of hybrid rocket motors more accurately. For this work, we focus on the atomization process as observed in a slab burner setup [10, 11]. One challenge with uncertainty quantification (UQ) of models that simulate the solid-liquid interface and

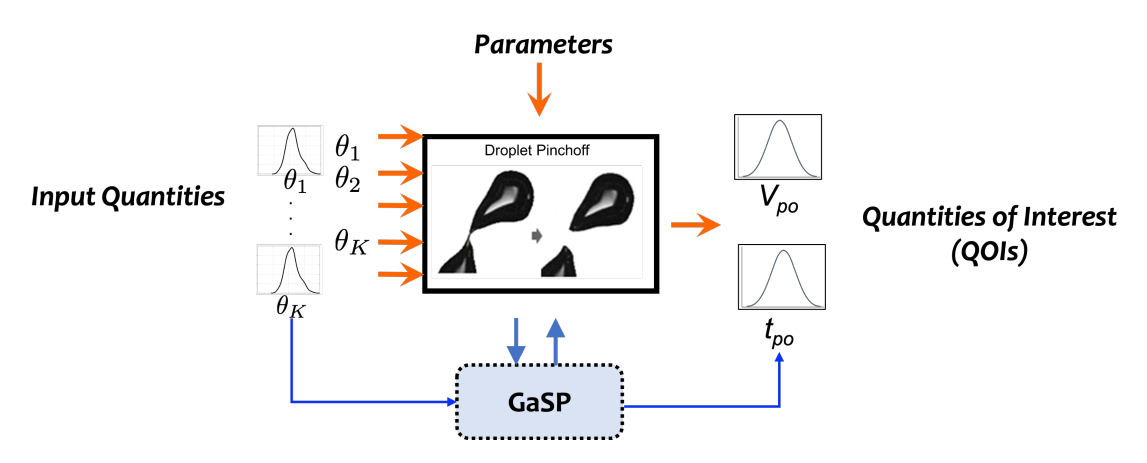


Fig. 2 Overview of the forward propagation of uncertainty using emulators such as Gaussian Processes (GaSP).

capture the atomization and pinch-off in detail is their computational cost. While costs allow simulating a few scenarios, it is infeasible for UQ that requires tens if not hundreds of thousands model evaluations to capture the statistics of the QoIs adequately. On a similar note, if one attempts to include detailed atomization models as components of a full turbulent combustion flow solver, the computational cost of the coupling is infeasible since we have to generate a very large number of droplets through these detailed atomization models. To work around these constraints, and before we proceed with uncertainty quantification of the pinch-off process, we develop a surrogate model (or emulator) for the shear-driven droplet pinch-off model. The surrogate used in this work is based on a Robust Gaussian Stochastic Process (GaSP) [12]. We then use the pinch-off surrogate to propagate forward uncertainty in the model inputs to the QoIs (V_{po} and t_{po}) via Monte-Carlo (MC) sampling methods [13]. Fig. 2 presents a summary of the forward UQ process. "Input quantities" are inputs and the main sources of uncertainty to the droplet pinch-off detailed model. "Parameters" are also inputs to the model, but are not considered uncertain, they often reflect some properties that are required by the model, but are fixed. Identification of inputs for UQ and parameters is often the result of a sensitivity calculation where only the dominant influences are retained in the input set. "Quantities of Interest" (QoIs) are the observable model outputs that we want to quantify the uncertainty of with a forward UQ process. Both the inputs and QoIs are represented as random variables, and their uncertainty is represented and quantified via probability distribution functions (PDFs).

To build the GaSP surrogate, we first generate an ensemble of 512 simulations of the droplet pinch-off model that cover appropriate ranges for the input quantities identified as the plausible and feasible values for those inputs including extreme values as appropriate. The inputs are sampled using Latin Hypercube Sampling (LHS) to ensure full exploration of the possible input space. After the surrogate is trained, we follow the approach demonstrated in Fig. 2 to estimate the posterior distributions (PDFs) of the pinch-off volume V_{po} and time t_{po} . Since the droplet atomization process is affected by gravity, we carry out 2 case studies to account for different gravity environments: Case (A) corresponds to a slab burner setup in the lab where the gravity term for the pinch-off model is equal to $a = -g = -9.81 \frac{m}{s^2}$ since the droplets are formed against Earth's gravity. Case (B) corresponds to the hypothetical scenario of a slab burner in space where a = 0, which would be applicable for a full hybrid rocket model.

The paper is organized as follows. Section II is an introduction to the droplet pinch-off phenomena in hybrid rocket motors and serves as the motivation for the work. Section III describes the mathematical model for shear-driven droplet pinch-off. Section IV presents the detailed process of inferring and computing the appropriate model inputs for the simulation ensemble used for training the GaSP surrogate. Section V describes Gaussian Processes, their use for UQ, and their training. Section VI includes the results and discussion. Section VII is the concluding section with directions for future work.

III. Pinch-off Physics Model

The basics of the droplet formation process can be understood with the example of a pendant droplet under gravity. Initially, there is a fluid column at the outlet of the nozzle. The fluid column becomes heavier by adding more fluid and gravity starts to pull it down, creating an elongated structure. Meanwhile, surface tension tries to minimize the

Quantity Symbol Description Type The oxidizer mass flux in the combustion chamber in $\frac{kg}{m^2s}$ Oxidizer mass flux GInput Inlet Velocity u_0^l Input Inlet velocity of a liquid droplet in m/sInlet Radius h_0 Inlet radius of a liquid droplet in m Input Fuel Density Density of the liquid layer in $\frac{kg}{m^3}$ ρ^l Input Kinematic Viscosity of the liquid layer in $\frac{m^2}{s}$ v^l Fuel Viscosity Input Fuel Surface Tension γ^l Surface tension of the liquid fuel – combustion gas interface in $\frac{kg}{c^2}$ Input Port radius R Parameter Port radius of the slab burner equal to 0.0254m Density of the oxidizer equal to $1 \frac{kg}{m^3}$ Oxidizer Density o^g Parameter Kinematic Viscosity of the oxidizer equal to $1.5e^{-5}\frac{m^2}{c}$ ν^g Oxidizer Viscosity Parameter The volume of a droplet that pinched off in m^3 Pinch-off Volume V_{po} OoI

Table 1 Quantities of the shear-driven droplet pinch-off model.

surface energy by changing the surface curvature. This process creates a neck with a rapidly decreasing radius. The radius of the fluid column eventually goes to zero and the droplet separates from the original fluid. The mathematical foundation for this process was laid in 1993 when Jens Eggers established a scaling solution of the axisymmetric fluid neck that appears in a droplet breakup process [14]. Eggers and Dupont [6] developed a one-dimensional mathematical model using the asymptotic expansion of the Navier-Stokes equations. Inspired by this previous work, we developed a one-dimensional (1-D) model to simulate the droplet pinch-off in a quiescent environment with accurate curvature using mixed finite element formulation and a self-consistent determination of droplet length [5].

QoI

 t_{po}

In a hybrid rocket combustion process, the droplet formation is driven by a shear force from the fast-moving combustion gas. We developed a novel mathematical model that is built using a pressure gradient-driven velocity description of the gas flow velocity. The input quantities and parameters for the shear-driven droplet model are summarized in Table 1.

The model equations are solved for u(z,t) (the velocity of the droplet at the interface) and h(z,t) (the radius of the droplet at the interface) and are given as follows.

$$\frac{\partial h}{\partial t} + u^l \frac{\partial h}{\partial z} + \frac{h}{2} \frac{\partial u^l}{\partial z} = 0 \tag{1}$$

$$\frac{\partial u^{l}}{\partial t} + u^{l} \frac{\partial u^{l}}{\partial z} + \frac{\gamma^{l}}{\rho^{l}} \frac{\partial \mathcal{K}}{\partial z} - \frac{6v^{l}}{h} \frac{\partial u^{l}}{\partial z} \frac{\partial h}{\partial z} \left(1 + \frac{\mu^{g}}{\mu^{l}} \right) - 3v^{l} \frac{\partial^{2} u^{l}}{\partial z^{2}} \left(1 + \frac{2}{3} \frac{\mu^{g}}{\mu^{l}} \right) + \frac{2}{\rho^{l}} \frac{dp^{g}}{dz} + \frac{1}{2\rho^{l} \ln(C)} \frac{dp^{g}}{dz} - \left(1 - \frac{\rho^{g}}{\rho^{l}} \right) g = 0$$
(2)

where, the K represents the full curvature, which is given by

Pinch-off Time

$$\mathcal{K} = \left[\frac{1}{h \left(1 + \frac{\partial h}{\partial z}^2 \right)^{1/2}} - \frac{\frac{\partial^2 h}{\partial z^2}}{\left(1 + \frac{\partial h}{\partial z}^2 \right)^{3/2}} \right]$$
(3)

The time it took for a particular droplet to pinch-off in s

The pressure gradient term (dp^g/dz) represents the pressure drop per unit length in the combustion gas flow. The parameter C depicts a measure of the shear layer thickness at the interface. The pressure gradient can be found using the oxidizer mass flux (G) and the port radius (R) using the following equation.

$$\frac{dp^g}{dz} = -\frac{8v^g G}{R^2} \tag{4}$$

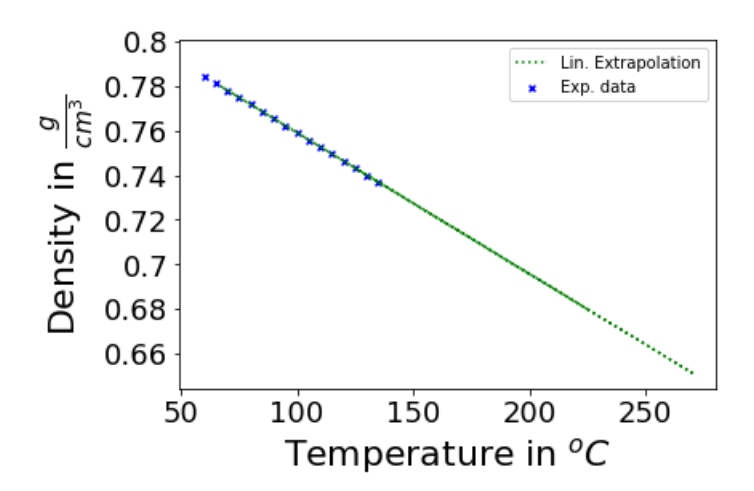


Fig. 3 Approximation of the density of paraffin with temperature from experimental data.

These equations are solved using a mixed finite element approach in order to accurately capture the curvature. We make use of adaptive mesh refinement, conservative Galerkin projection between moving meshes, and a self-consistent algorithm to compute droplet length. The implementation makes use of the PETSc library [15, 16].

IV. Derivation of Input Parameters for the Gaussian Process

Some of the input quantities to the pinch-off model (Table 1) are not independent and are derived directly from the conditions in the combustion chamber. More specifically, the temperature of the paraffin liquid layer T^l defines the density ρ^l , the viscosity v^l , and the surface tension γ^l . The wavelength of the formed instability layer λ^l defines the inlet radius h_0 . The corresponding regression rate for the oxidizer flux G and the wavelength λ^l both define the droplet formation inlet velocity u_0^l . If we were to sample ρ^l , v^l , γ^l independently as inputs, we would be misrepresenting the correct material properties for the paraffin fuel. For these reasons, the inputs to the GaSP surrogate are the underlying independent quantities for the pinchoff model: the temperature of the liquid layer T^l , the wavelength of the formed instability λ^l , and the oxidizer flux G.

To derive the input quantities in Table 1 from the underlying independent quantities T^l , λ^l , G, we rely primarily on experimental evidence from the literature with appropriate approximations. The main challenge with the process is that experimental data cover a small range for the temperature (up to $135^{\circ}C$) of paraffin, and extrapolation is necessary for our simulation ensemble (up to $270^{\circ}C$). Therefore, the following approximations are chosen based on the quality of their extrapolations.

The density of the paraffin is linearly modeled to the temperature based on experimental data collected by [17] and is shown in Fig. 3. The experimental data include measurements of the density of paraffin from $60^{\circ}C$ to $135^{\circ}C$.

$$\rho^l = -6.32e^{-4}T^l + 0.82 \tag{5}$$

With T^l measured in $[{}^oC]$ and ρ^l in $[\frac{g}{cm^3}]$. The kinematic viscosity is modeled with a regression fit to a modified Arrhenius equation [18] as follows:

$$\log(\frac{v^{l}}{v_{ref}^{l}}) = A + B \frac{T_{ref}^{l}}{T^{l}} + C(\frac{T_{ref}^{l}}{T^{l}})^{2} + D(\frac{T_{ref}^{l}}{T^{l}})^{3}$$
(6)

Where $T_{ref}^l = 373.15K(100^oC)$, and $v_{ref}^l = 4.12\frac{mm^2}{s}$ the kinematic the viscosity of paraffin at the reference temperature. Fig. 4 shows the results of the modified Arrhenius fit with the experimental data collected from [17]. The parameters of the fit are: A = 0, B = -7.09, C = 8.06, D = -1.09.

The surface tension of the paraffin was studied thoroughly by [19] and [20] and they found a linear model of the temperature is adequate:

$$\gamma^l = -0.07T^l + 35.2 \tag{7}$$

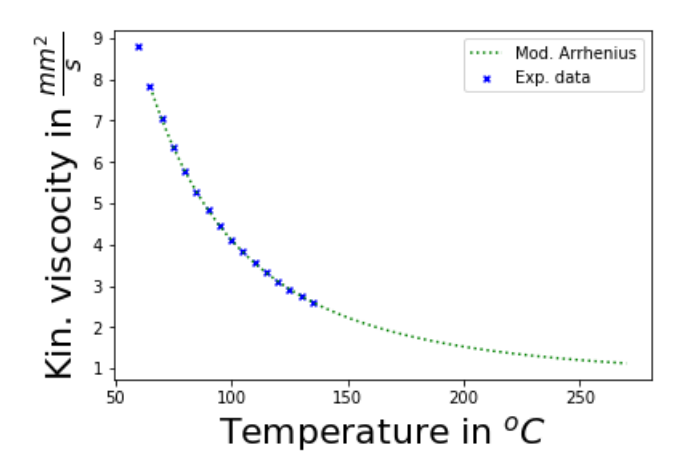


Fig. 4 Approximation of the kinematic viscosity of paraffin with temperature from experimental data using a modified Arrhenius equation.

With T^l measured in $[{}^oC]$ and γ^l in $[\frac{mN}{m}]$.

Apart from the material properties for the paraffin wax, the inlet radius h_0 and inlet velocity u_0^l for the pinch-off model are dependent on the wavelength of the instability layer λ^l and/or the corresponding regression rate \dot{r} for a given G. Therefore, the inlet radius is defined as a fourth of the wavelength, assuming the crest of the wave to be a nucleation site for a droplet to form:

$$h_0 = \frac{\lambda^l}{4} \tag{8}$$

Assuming that the width of the slab burner is much smaller than its length $(W \ll L)$, the instabilities are mostly along its length L, and that the total volume of droplets exiting the liquid is equal to the volume regression of the solid fuel, the inlet velocity can be derived as follows:

Droplet pinch-off volume rate = Volume regression rate

No. of pinch-off locations $\times \pi h_0^2 u_0^l = W L \dot{r}$

$$\left(\frac{L}{\lambda^l}\right) \times \pi h_0^2 u_0^l = W L \dot{r}$$

$$u_0^l = \frac{16W \dot{r}}{\lambda^l \pi} \qquad (\because h_0 = \frac{\lambda^l}{4})$$

The regression rate \dot{r} for a given G is approximated based on [21].

Given the aforementioned formulations, a design point $x_i^d = [T_i^l, \lambda_i^l, G_i]$ in the 512 simulation ensemble has an equivalent $x_{im} = [\rho_i^l, \nu_i^l, \gamma_i^l, h_0, u_0^l, G_i]$ as input to the pinch-off model. To generate the ensemble, T_i^l, λ_i^l, G_i are sampled with Latin Hypercube Sampling (LHS). LHS is defined as a sampling method where each sample is the only one in each axis-aligned hyperplane containing it. Fig. 5 shows the LHS for our case. After the ensemble simulations are complete, we used the independent inputs $x^d = [x_1^d, x_2^d, ..., x_{512}^d]$ and corresponding pinch-off model outputs $y^d = [y_1^d, y_2^d, ..., y_{512}^d]^T$ to train the GaSP emulator as described in the following Section V.

V. Uncertainty Quantification with Gaussian Processes

In this section, we provide background into the GaSP used in this paper, and how these emulators are used for UQ. Our approach here builds on a Gaussian process with robust parameter estimation, as developed by Gu et al. ([12]). Gaussian processes for UQ are not new, but new adaptations and applications of them on aerospace problems continue to appear in the literature. Recently for example, Fu et al. ([22]) developed a method for updating a GaSP model in the augmented space of aleatory and epistemic parameters and demonstrated its use in the dynamic reliability analysis of a satellite structure. Ignatyev et al. ([23]) presented a sparse online GaSP for flight control. GaSP are preferred to use as

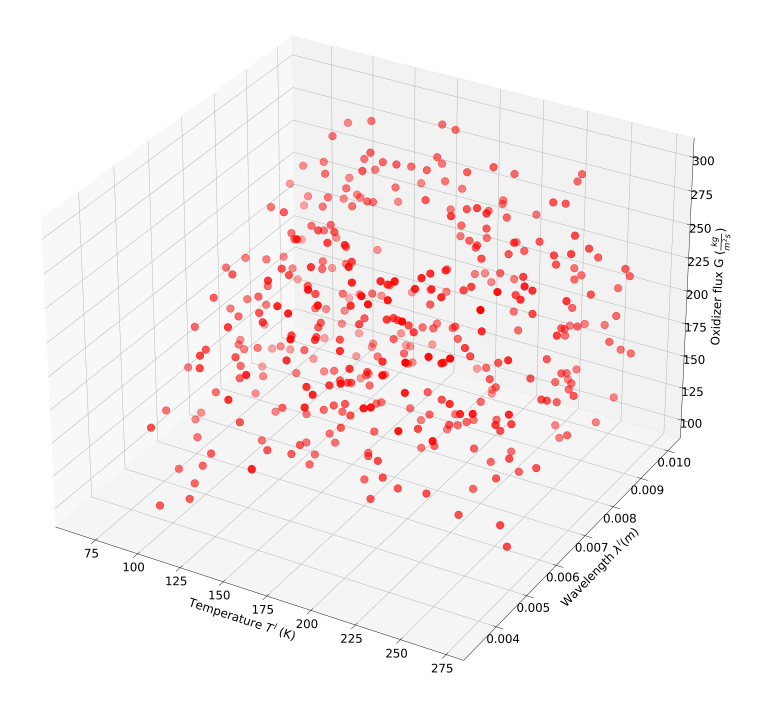


Fig. 5 Latin Hypercube Sampling (LHS) of inputs temperature (T_i^l) , wavelength (λ_i^l) , and oxidizer flux (G_i) for the 512 simulation ensemble to generate the training set for the surrogate model training.

emulators because they are fast, and therefore allow for UQ analyses of expensive computational models to be feasible. As a point of comparison, one full simulation of one output from the detailed pinch-off model we used in this paper takes on average 5-10 minutes, whereas the GaSP emulator $6.87\mu s$. Training the GaSP takes about 0.15s. GaSP are also more explainable [24] and can successfully be used for global sensitivity analyses [25], unlike less interpretable alternatives like neural nets.

GaSP assumes that the likelihood function of the QoI is a multivariate normal distribution (Eq. 9).

$$[y(x_1), y(x_2), ..., y(x_n)]^T \approx \mathcal{MN}([\mu(x_1), \mu(x_2), ..., \mu(x_n)]^T, \sigma^2 \mathbf{R})$$
 (9)

Where $y(\cdot)$ is the real-valued QoI output, $x^d \in X$ is the input vector of d-dimension (here d = 3), $\mu(\cdot)$ is the mean function, σ^2 is the unknown variance, and R is the correlation matrix.

The mean function $\mu(\cdot)$ of a GaSP is typically modeled as a regression:

$$\mu(\mathbf{x}) = \sum_{i=1}^{q} h_i(\mathbf{x})\theta_i \tag{10}$$

Where $h_i(\cdot)$ are the mean basis functions and θ_i the corresponding regression coefficients. It is often chosen, as we also do in this paper, for the mean basis functions to be constant, i.e., $h_i(x) = 1$.

The elements of the correlation matrix R in eq. 9, are the values of a chosen correlation function between observation vectors x_i, x_j :

$$c(\mathbf{x}_i, \mathbf{x}_j) = \prod_{k=1}^d c_k(x_{ik}, x_{jk})$$

$$\tag{11}$$

Where c_k is the output of the correlation function for the k^{th} coordinate of the two input vectors. There are many options for correlation functions and here we use the Matérn kernel because its smoothness can be tuned based on the roughness parameter α , which allows for more flexibility [26]:

$$\frac{1}{2^{\alpha-1}\Gamma(\alpha)} \left(\frac{d}{\gamma}\right)^{\alpha} \mathcal{K}_{\alpha} \left(\frac{d}{\gamma}\right) \tag{12}$$

Algorithm 1: Estimation of the distribution of the QoIs of droplet pinch-off

Assume uniform distribution for:

 $T^l \sim \mathcal{U}(T_{min} = 66^{\circ}C, T_{max} = 270^{\circ}C)$. $66^{\circ}C$ is the evaporation temperature, and $270^{\circ}C$ is the boiling

 $\lambda^{l} \sim \mathcal{U}(1/100, 1/300)$. These are estimates of the instability layer for a 10cm long slab burner.

 $G \sim \mathcal{U}(100, 300) \frac{kg}{m^2s}$. Oxidizer flux is picked as such to simulate a range where pinch-off effects are dominant. **While** $\|\frac{\sigma_{Vpo,tpo}^{2,new} - \sigma_{Vpo,tpo}^{2,old}}{\sigma_{Vpo,tpo}^{2,old}}\| > e^{-5}$ **do**: Step 1. Draw N = 1000 samples from each of the input quantities to create design vectors

While
$$\|\frac{\sigma_{Vpo,tpo}^{2,new} - \sigma_{Vpo,tpo}^{2,old}}{\sigma_{Vpo,tpo}^{2,old}}\| > e^{-5}$$
 do

$$\mathbf{x}_{i..N}^* = [T_{i..N}^{l*}, \lambda_{i..N}^{l*}, G_{i..N}^*]$$

 $\begin{aligned} \boldsymbol{x}_{i..N}^* &= [T_{i..N}^{l*}, \lambda_{i..N}^{l*}, G_{i..N}^*] \\ & \textit{Step 2. Pass the new design vector to the GaSP to get the prediction } \boldsymbol{y}(\boldsymbol{x}_{i..N}^*) = (V_{po}^*, t_{po}^*)_{i..N}^T \end{aligned}$

Step 3. Append probability distributions $p(V_{po}) = +(V_{po}^*)_{i..N}$, and $p(t_{po}) = +(t_{po}^*)_{i..N}$. Step 4. Update variances $\sigma_{V_{po}}^{2,new}$, $\sigma_{t_{po}}^{2,new}$

End While

Where $0 < \alpha < 1$ is the roughness parameter, γ is the range parameter, $\Gamma(\cdot)$ is the gamma function, $\mathcal{K}_{\alpha}(\cdot)$ is the modified Bessel function, and $d = |x_{ik}, x_{ik}|$.

Overall, the unknown parameters in the GaSP formulation include the regression coefficients θ , the variance σ^2 , and the range parameters from the kernel as a vector γ . In this formulation, the marginal likelihood function after integrating out (θ, σ^2) becomes:

$$\mathcal{L}(y^d|\mathbf{y}) \propto |\mathbf{R}|^{-1/2} |\mathbf{h}^T(\mathbf{x}^d) \mathbf{R}^{-1} \mathbf{h}^T(\mathbf{x}^d)|^{-1/2} (S^2)^{-(\frac{n-q}{2})}$$
(13)

Where $S^2 = (y^d)^T Q y^d$, $Q = R^{-1} P$, and $P = I_n - h(x^d) [h^T (x^d) R^{-1} h(x^d)]^{-1} h^T (x^d) R^{-1}$. I_n is the identity matrix of size n = 512, which is equal to the number of simulation observations.

The range parameters γ are then estimated by the modes of the marginal posterior distribution:

$$\hat{\gamma} = argmax_{(\gamma_1, \dots, \gamma_p)} \mathcal{L}(y^d | \gamma) \pi(\gamma_1, \dots, \gamma_p)$$
(14)

To train the GaSP, we use the aforementioned design points $(x^d = [x_1^d, x_2^d, ..., x_{512}^d])$ and the outputs of the pinch-off model at these points $(y^d = [y_1^d, y_2^d, ..., y_{512}^d]^T)$ for the parameter estimation described above. After training, the GaSP can be used for prediction at a new point $x^* = [T^{l*}, \lambda^{l*}, G^*]$.

To complete the forward UQ process, which will result in the statistics of the droplet pinch-off QoIs, we used a Monte-Carlo sampling method after assuming uniform distribution for the inputs (Alg. 1). After the algorithm has converged, we obtain the resulting probability distribution for the QoIs and therefore, any relevant statistics for the QoIs.

VI. Results and Discussion

After training the GaSP as described in Section V, we studied the overall quality of the surrogate model by investigating the prediction accuracy at the training points for the two cases (Case A with gravity effects shown in Fig. 6 and Case B without gravity effects shown in Fig. 7).

For both cases we come up with similar conclusions. Firstly, we observe that the wavelength is the most important parameter for defining the pinch-off volume as evident by the strong trend, which is expected since the wavelength defines the droplet size directly based on our formulation. For the pinch-off time, we do observe a trend of larger wavelengths corresponding to longer pinch-off times, which is expected given that these wavelengths mean larger (and therefore heavier) droplets. However, for pinch-off time and unlike what we observed for the pinch-off volume, all 3 input parameters are important. Overall, the GaSP appears to be an acceptable surrogate for the underlying expensive model, evident by the predictions being close to the actual simulation data with some error.

Then, we study the association between the prediction errors at training points as a function of each input variable (Case A with gravity effects shown in Fig. 8 and Case B without gravity effects shown in Fig. 9). For both cases, we observe that when predicting pinch-off volume, there is a trend of smaller wavelengths corresponding to higher errors and all 5 outliers are in that range. Overall, the surrogate reliably predicts pinch-off volume within 10% accuracy, and the errors appear uniformly distributed throughout temperature and oxidizer flux range. When predicting pinch-off time, there is some concentration of outliers towards larger wavelengths, but overall the errors are uniformly distributed

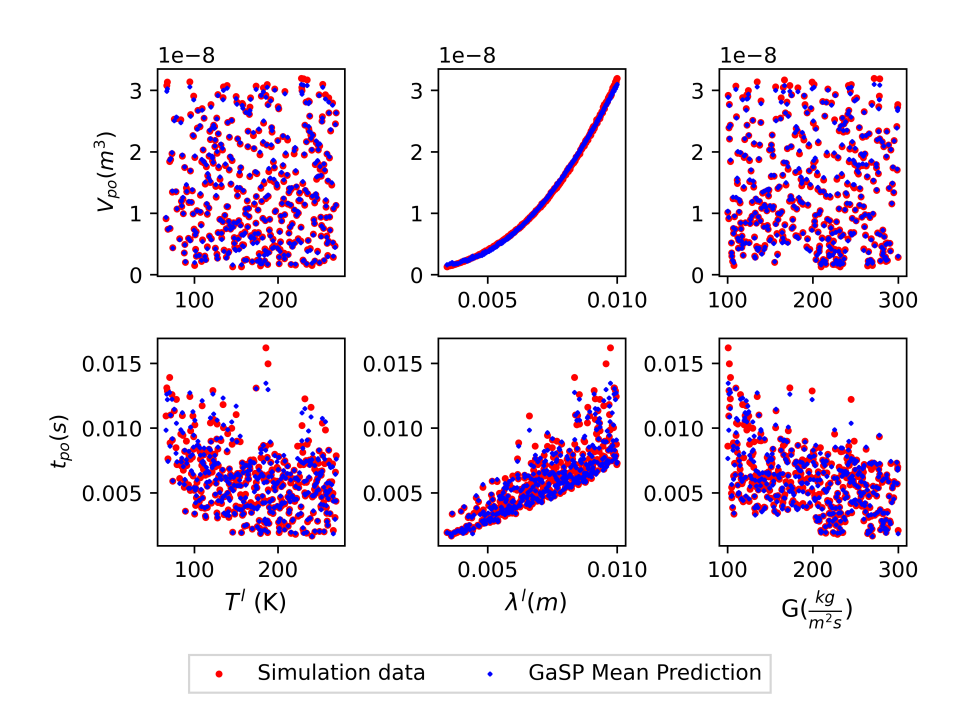


Fig. 6 Case A (with gravity effects): Overall, we find that GaSP produces a good surrogate model for both QoIs. The pinch-off volume appears to be mostly defined by the wavelength as evident by the strong trend. For the pinch-off time, all 3 inputs appear to be important.

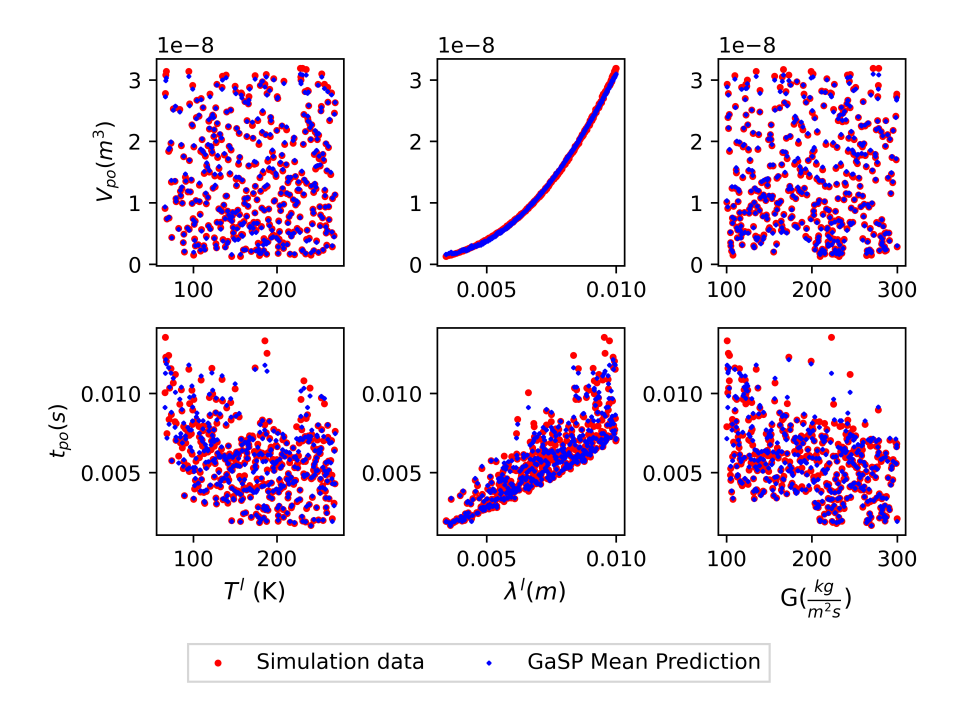


Fig. 7 Case B (no gravity effects): Overall, we find that GaSP produces a good surrogate model for both QoIs. Pinch-off volume appears to be mostly defined by the wavelength as evident by the strong trend. For the pinch-off time, all 3 inputs appear to be important.

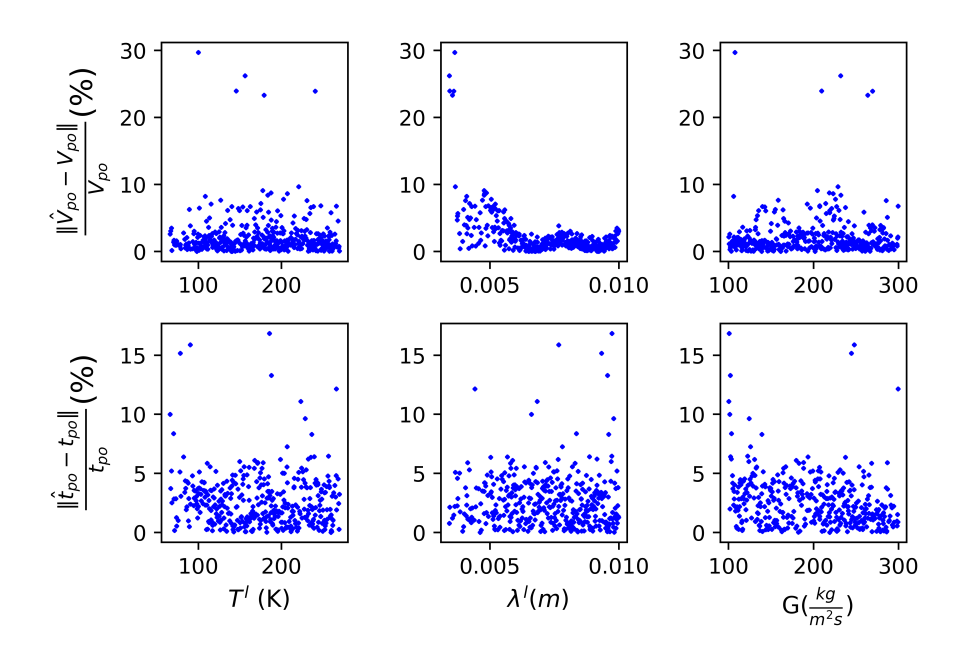


Fig. 8 Case A (with gravity effects): Further investigation of percentage error between surrogate prediction and simulation data, for different values of the inputs.

For pinch-off volume: the surrogate predicts within 10% percentage error apart from 5 outlier points at very low wavelengths. In general, error distributions appear uniform throughout the range of temperatures and oxidizer fluxes. There is a trend of larger errors at smaller wavelengths.

For pinch-off time: the majority of points are within 5% prediction accuracy with outliers at various ranges of the inputs. Overall the errors appear uniformly distributed throughout the input range.

throughout the range of all input parameters. The surrogate (excluding 10 outlier points) reliably predicts pinch-off time within 5% accuracy.

For completion and further comparison, we have randomly selected 12 training points and present the inputs, surrogate prediction, the true values from simulation, and the corresponding for the two cases and QoIs. For Case A with gravity effects see Table 4 for pinch-off volume and Table 5 for pinch-off time. For Case B without gravity effects see Table 6 for pinch-off volume and Table 7 for pinch-off time.

Also, we carried out a validation study where we leave out 10 simulation points to estimate the accuracy of the GaSP at these points that were not part of the training. The results of this process are shown in Table 2 and 3.

We conclude that overall, the surrogate models are adequate in this case and could be used as emulators of the true physical model after investigating the outliers at very small wavelengths (for pinch-off volume) and larger wavelengths (for pinch-off time).

Lastly, we present the resulting probability distributions for the QoIs under the two cases after using the GaSP surrogate to forward propagate the uncertainty in the inputs (assumed uniform) as described in Alg. 1.

Fig. 10 and Fig. 11 correspond to case A with gravity effects. Both QoIs have right-skewed distributions, with higher densities at smaller pinch-off volumes and times. Despite the uniformly sampled wavelength being the dominant factor in pinch-off volume, we observe that model predictions concentrate towards smaller pinch-off volume areas. The pinch-off time also has a higher probability density towards smaller times, which is also similar to what we observed during the training of the model with our ensemble(i.e., fewer occurrences of long pinch-off times, mostly corresponding to large wavelengths in low oxidizer flux environments).

Fig. 12 and Fig. 13 correspond to Case (B) without gravity effects. Both QoIs have right-skewed distributions, with higher densities at smaller pinch-off volumes and times, similar to Case A. Comparing the two cases, the pinch-off volume appears to be unaffected by gravity effects, given that it is mostly dependent on the wavelength (Fig. 14). However, in the absence of gravity effects (Case B) we observe the pinch-off times are shorter (Fig. 15) than when gravity effects are present (Case A), which is an expected result. Earth's gravity acts against the direction where droplet

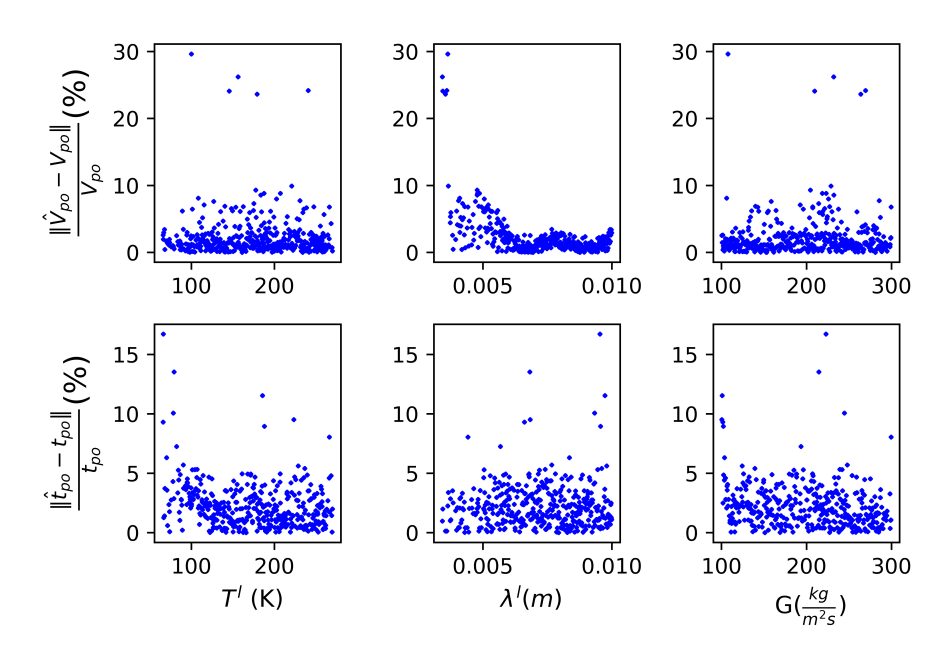


Fig. 9 Case B (no gravity effects): Further investigation of percentage error between surrogate prediction and simulation data, based on different values of the inputs. We make the same conclusions as Case A (see Fig. 8).

Table 2 Validation of GaSP for predicting pinch-off volume at 10 simulation points that are withheld from training (data from Case B).

$T^l({}^oC)$	$\lambda^l(m)$	$G\frac{kg}{m^2s}$	$GaSP(\mu,\sigma)(10^{-9}m^3)$	True $V_{po}(10^{-9}m^3)$	$\frac{\ \hat{V}_{po} - V_{po}\ }{V_{po}}$ (%)
257.893	0.006	266.697	(9.321, 0.539)	9.32	0.011
117.192	0.007	144.728	(10.923, 0.312)	10.9	0.211
117.436	0.008	153.151	(19.507, 0.329)	19.3	1.073
179.064	0.004	263.955	(1.606, 0.674)	1.44	11.528
259.765	0.008	270.816	(15.367, 0.584)	15.2	1.099
176.091	0.007	237.369	(10.586, 0.296)	10.5	0.819
223.412	0.007	100.347	(10.363, 0.590)	10.1	2.604
216.960	0.006	156.580	(8.174, 0.323)	8.33	1.873
220.830	0.004	228.786	(1.739, 0.630)	1.57	10.764
100.137	0.004	107.616	(1.978, 1.009)	1.725	14.667

Table 3 Validation of GaSP for predicting pinch-off time at 10 simulation points that are withheld from training (data from Case B).

$T^l({}^oC)$	$\lambda^l(m)$	$G\frac{kg}{m^2s}$	GaSP $(\mu, \sigma)(ms)$	True $t_{po}(ms)$	$\frac{\ \hat{t}_{po} - t_{po}\ }{t_{po}} (\%)$
257.893	0.006	266.697	(3.969, 0.193)	3.830	3.629
117.192	0.007	144.728	(6.400, 0.116)	6.303	1.539
117.436	0.008	153.151	(8.149, 0.122)	8.030	1.482
179.064	0.004	263.955	(1.850, 0.253)	1.852	0.108
259.765	0.008	270.816	(4.963, 0.215)	4.877	1.763
176.091	0.007	237.369	(4.445, 0.107)	4.599	3.349
223.412	0.007	100.347	(7.074, 0.223)	7.902	10.478
216.960	0.006	156.580	(4.711, 0.114)	4.637	1.596
220.830	0.004	228.786	(1.861, 0.225)	1.792	3.850
100.137	0.004	107.616	(3.399, 0.379)	3.319	2.410

Table 4 Case A (with gravity effects): Quality of surrogate fit for pinch-off volume V_{po} at 12 randomly selected training points. The average percentage error among all training points is 2.266%.

$T^l(^oC)$	$\lambda^l(m)$	$G\frac{kg}{m^2s}$	$GaSP(\mu,\sigma)(10^{-9}m^3)$	True $V_{po}(10^{-9}m^3)$	$\frac{\ \hat{V}_{po} - V_{po}\ }{V_{po}}$ (%)
117.192	0.006	144.72	(10.922, 0.309)	10.856	0.604
160.431	0.006	205.91	(6.8, 0.296)	6.972	2.462
164.056	0.008	286.38	(23.284, 0.464)	23.367	0.353
150.969	0.007	205.75	(14.217, 0.294)	13.868	2.519
212.952	0.005	275.64	(6.685, 0.386)	6.815	1.907
114.294	0.008	253.8	(17.885, 0.375)	17.581	1.725
211.382	0.008	189.3	(22.376, 0.314)	21.922	2.072
94.572	0.009	134.71	(30.556, 0.715)	31.382	2.633
193.253	0.005	116.62	(4.285, 0.547)	4.447	3.635
128.571	0.008	265.72	(22.987, 0.406)	22.917	0.307
87.893	0.004	104.84	(3.566, 0.736)	3.536	0.841
169.103	0.004	269.24	(2.176, 0.574)	2.094	3.954

Table 5 Case A (with gravity effects): Quality of surrogate fit for pinch-off time t_{po} at 12 randomly selected training points. The average percentage error among all training points is 2.65%.

$T^l({}^oC)$	$\lambda^l(m)$	$G\frac{kg}{m^2s}$	GaSP $(\mu, \sigma)(ms)$	True $t_{po}(ms)$	$\frac{\ \hat{t}_{po} - t_{po}\ }{t_{po}} (\%)$
117.192	0.006	144.72	(6.537, 0.13)	6.498	0.602
160.431	0.006	205.91	(3.946, 0.12)	4.105	3.868
164.056	0.008	286.38	(6.4, 0.169)	6.393	0.111
150.969	0.007	205.75	(5.545, 0.116)	5.85	5.212
212.952	0.005	275.64	(3.495, 0.154)	3.434	1.781
114.294	0.008	253.8	(6.973, 0.139)	6.606	5.554
211.382	0.008	189.3	(7.048, 0.132)	7.086	0.539
94.572	0.009	134.71	(12.719, 0.308)	12.438	2.259
193.253	0.005	116.62	(4.497, 0.239)	4.485	0.268
128.571	0.008	265.72	(7.281, 0.141)	7.114	2.34
87.893	0.004	104.84	(5.647, 0.282)	5.421	4.17
169.103	0.004	269.24	(2.236, 0.221)	2.202	1.553

Table 6 Case B (no gravity effects): Quality of surrogate fit for pinch-off volume V_{po} at 12 randomly selected training points. The average percentage error among all training points is 2.265%.

$T^l(^oC)$	$\lambda^l(m)$	$G\frac{kg}{m^2s}$	$GaSP(\mu,\sigma)(10^{-9}m^3)$	True $V_{po}(10^{-9}m^3)$	$\frac{\ \hat{V}_{po} - V_{po}\ }{V_{po}} (\%)$
259.764	0.007	270.816	(15.368, 0.556)	15.2	1.105
86.712	0.006	159.396	(9.978, 0.402)	9.94	0.382
164.056	0.008	286.383	(23.28, 0.463)	23.4	0.512
194.379	0.008	247.349	(18.62, 0.292)	18.299	1.754
77.942	0.007	208.632	(13.636, 0.49)	13.5	1.007
233.938	0.008	281.120	(21.6, 0.526)	21.6	0
236.524	0.009	139.178	(27.839, 0.533)	28.299	1.625
71.520	0.008	136.661	(18.948, 0.567)	18.699	1.331
93.367	0.007	128.939	(11.948, 0.411)	11.799	1.262
212.108	0.004	281.570	(3.215, 0.478)	3.309	2.84
242.150	0.005	245.403	(6.452, 0.378)	6.629	2.67
90.730	0.007	212.305	(13.573, 0.405)	13.5	0.54

Table 7 Case B (no gravity effects): Quality of surrogate fit for pinch-off time t_{po} at 12 randomly selected training points. The average percentage error among all training points is 2.277%.

$T^l({}^oC)$	$\lambda^l(m)$	$G\frac{kg}{m^2s}$	GaSP $(\mu, \sigma)(ms)$	True $t_{po}(ms)$	$\frac{\ \hat{t}_{po} - t_{po}\ }{t_{po}} (\%)$
259.764	0.007	270.816	(4.949, 0.201)	4.877	1.476
86.712	0.006	159.396	(6.886, 0.141)	6.565	4.889
164.056	0.008	286.383	(6.227, 0.151)	6.244	0.272
194.379	0.008	247.349	(5.647, 0.11)	5.781	2.317
77.942	0.007	208.632	(7.863, 0.183)	8.217	4.308
233.938	0.008	281.12	(5.837, 0.187)	5.712	2.188
236.524	0.009	139.178	(9.116, 0.176)	8.649	5.399
71.520	0.008	136.661	(10.4, 0.201)	10.339	0.589
93.367	0.007	128.939	(7.849, 0.138)	7.575	3.617
212.108	0.004	281.57	(2.456, 0.157)	2.417	1.613
242.150	0.005	245.403	(3.53, 0.135)	3.436	2.735
90.730	0.007	212.305	(7.13, 0.141)	6.873	3.739

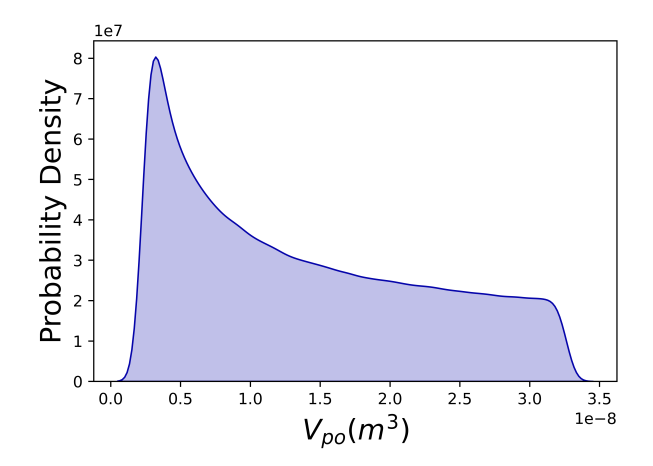


Fig. 10 Case A (with gravity effects): Probability distribution of the pinch-off volume V_{po} , which appears to be a right-skewed distribution. Our further analysis has revealed that despite a direct relationship between wavelength and pinch-off time, uniformly sampling inputs result in larger probability density towards smaller pinch-off volumes.

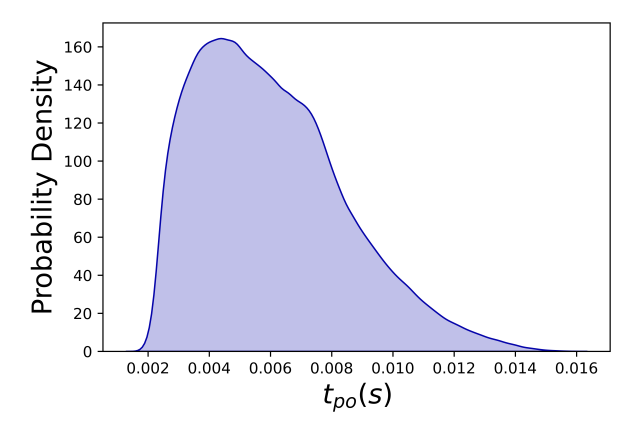
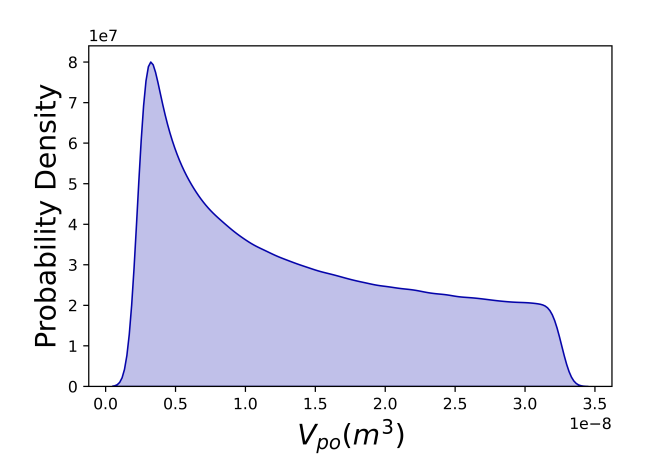


Fig. 11 Case A (with gravity effects): Probability distribution of the pinch-off time t_{po} , which appears to be a right-skewed distribution. The result is in agreement with our expectation, longer than 0.01s pinch-off times are a rarer occurrence, corresponding to large wavelengths in low oxidizer flux environments (smaller shear force).



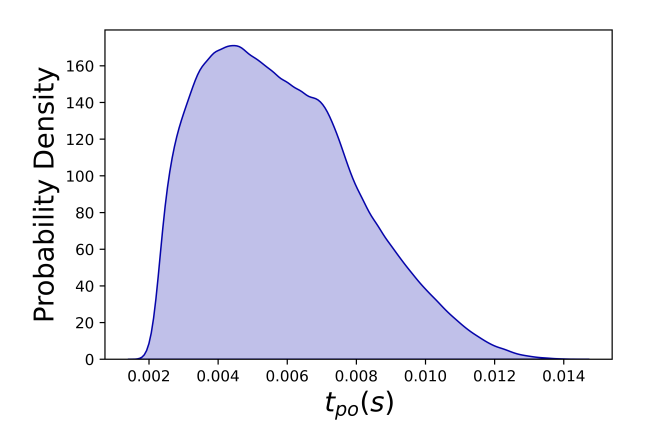


Fig. 12 Case B (no gravity effects): Probability distribution of the pinch-off volume V_{po} , which appears to be a right-skewed distribution.

Fig. 13 Case B (no gravity effects): Probability distribution of the pinch-off time t_{po} , which appears to be a right-skewed distribution.

formation and pinch-off occurs, resulting in the right-tail of the distribution reflecting longer pinch-off times compared to the case where there is no gravity.

VII. Conclusions and Future Work

The goal of this paper was to quantify the uncertainty associated with droplet pinch-off and its quantities of interest (QoIs): the pinch-off volume (V_{po}) and time (t_{po}) under different gravity conditions. Case A corresponded to the case of a slab burner in the lab with Earth's gravity acting against the droplet formation process, and Case B to a case in space where gravity is not present. We presented a first principles mathematical model that describes droplet formation under external forcing. The model simulates the formation and pinch-off of a droplet from the liquid paraffin layer, under shearing effects of the fast moving combustion gas.

To complete the UQ analysis, we developed a Gaussian Process (GaSP) surrogate for the first principles model, which we trained on a 512 simulation ensemble by appropriately sampling the underlying input variables: temperature of the liquid layer T^l , wavelength of the instability λ^l , and oxidizer flux G. We concluded that the GaSP is an acceptable surrogate for the pinch-off model and reliably predicts pinch-off volume within 10% accuracy and pinch-off time within 5% accuracy at the training points.

After forward-propagating the uncertainty of the inputs using the GaSP surrogate, we found the resulting probability distributions for the QoIs. We concluded that both QoIs have right-skewed distributions, with higher densities at smaller pinch-off volumes and times. Specifically, for the pinch-off times, the resulting distributions reflect the effect of gravity acting against droplet formation, resulting in longer pinch-off times compared to the case where there is no gravity.

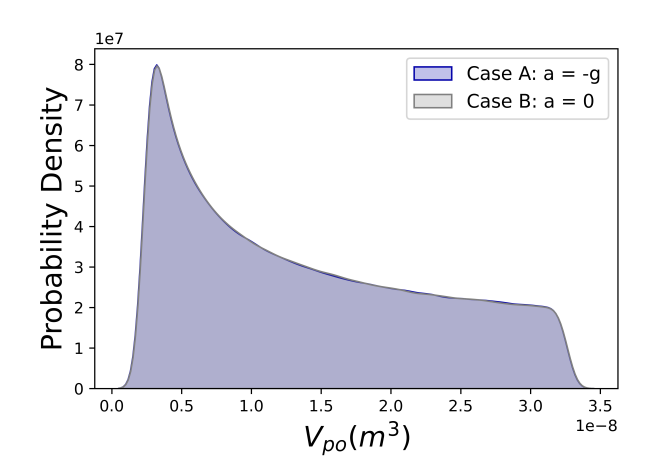
In future work, we aim to study whether approximating the pinch-off process with emulators as shown here, and coupling their output with a turbulent combustion solver (i.e., treating the droplet forming and atomization stochastically), yields equivalent results to modeling the droplet formation with detailed descriptions at the fuel-oxidizer interface layer, within a combustion flow solver.

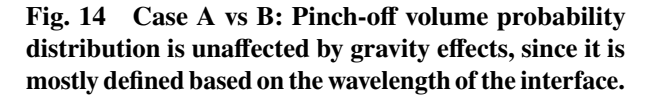
Acknowledgments

This work was supported by the United States Department of Energy's (DoE) National Nuclear Security Administration (NNSA) under the Predictive Science Academic Alliance Program III (PSAAP III) at the University at Buffalo, under contract number DE-NA0003961.

References

[1] Jens, E. T., Cantwell, B. J., and Hubbard, G. S., "Hybrid rocket propulsion systems for outer planet exploration missions," *Acta Astronautica*, Vol. 128, 2016, pp. 119–130. https://doi.org/https://doi.org/10.1016/j.actaastro.2016.06.036.





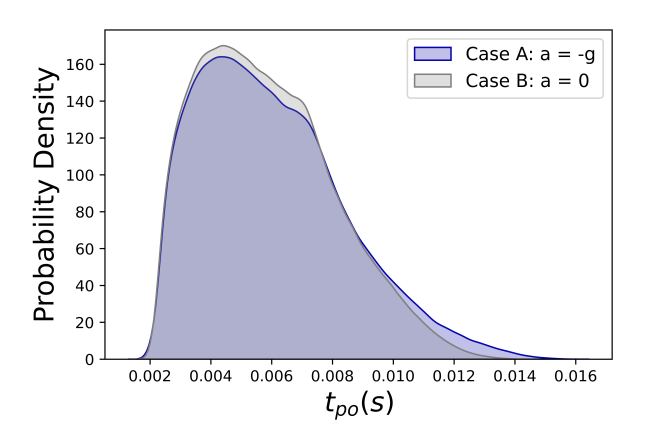


Fig. 15 Case A vs B: Earth's gravity acts against the direction where droplet formation and pinch-off occurs, resulting in the right-tail of the distribution being longer pinch-off times for Case A, compared to the case where there is no gravity.

- [2] Carrick, P., and Larson, C., "Lab scale test and evaluation of cryogenic solid hybrid rocket fuels," *In 31st Joint Propulsion Conference and Exhibit*, 1995, p. 2948. https://doi.org/10.2514/6.1995-2948.
- [3] Sementilli, M., Schulwitz, M., Pakseresht, P., and Chen, J., "Influence of vortex-shedding on interfacial instabilities in hybrid rocket fuel liquid layers," *In AIAA SCITECH 2022 Forum*, 2022, p. 2230. https://doi.org/https://doi.org/10.2514/6.2022-2230.
- [4] Karabeyoglu, M., Altman, D., and Cantwell, B., "Combustion of liquefying hybrid propellants: Part 1, general theory," *Journal of Propulsion and Power*, Vol. 18 (3), 2012, pp. 610–620. https://doi.org/https://doi.org/10.2514/2.5975.
- [5] Nathawani, D. K., and Knepley, M. G., "Droplet formation simulation using mixed finite elements," *Physics of Fluids*, Vol. 34, No. 6, 2022. https://doi.org/10.1063/5.0089752.
- [6] Eggers, J., and Dupont, T. F., "Drop formation in a one-dimensional approximation of the Navier–Stokes equation," *Journal of Fluid Mechanics*, Vol. 262, 1994, p. 205–221. https://doi.org/10.1017/S0022112094000480.
- [7] Yoon, S. S., and Heister, S. D., "A nonlinear atomization model based on a boundary layer instability mechanism," *Physics of Fluids*, Vol. 16, No. 1, 2003, pp. 47–61. https://doi.org/10.1063/1.1629301.
- [8] Gorokhovski, M., and Herrmann, M., "Modeling Primary Atomization," *Annual Review of Fluid Mechanics*, Vol. 40, No. 1, 2008, pp. 343–366. https://doi.org/10.1146/annurev.fluid.40.111406.102200.
- [9] Nathawani, D., and Knepley, M., "Simulating Paraffin Wax Droplets Using Mixed Finite Element Method," *ICCFD 11 PROCEEDINGS*, 2022.
- [10] Dunn, C., Gustafson, G., Edwards, J., Dunbrack, T., and Johansen, C., "Spatially and temporally resolved regression rate measurements for the combustion of paraffin wax for hybrid rocket motor applications," *Aerospace Science and Technology*, Vol. 72, 2018, pp. 371–379. https://doi.org/https://doi.org/10.1016/j.ast.2017.11.024.
- [11] Surina, G., Georgalis, G., Aphale, S. S., Patra, A., and DesJardin, P. E., "Measurement of hybrid rocket solid fuel regression rate for a slab burner using deep learning," *Acta Astronautica*, Vol. 190, 2022, pp. 160–175. https://doi.org/https://doi.org/10.1016/j.actaastro.2021.09.046.
- [12] Gu, M., Wang, X., and Berger, J. O., "ROBUST GAUSSIAN STOCHASTIC PROCESS EMULATION," *The Annals of Statistics*, Vol. 46, No. 6A, 2018, pp. 3038–3066.
- [13] Zhang, J., "Modern Monte Carlo methods for efficient uncertainty quantification and propagation: A survey," *WIREs Computational Statistics*, Vol. 13, No. 5, 2021, p. e1539. https://doi.org/https://doi.org/10.1002/wics.1539.
- [14] Eggers, J., "Universal pinching of 3D axisymmetric free-surface flow," Physical Review Letters, Vol. 71, No. 21, 1993, p. 3458.

- [15] Balay, S., Abhyankar, S., Adams, M. F., Benson, S., Brown, J., Brune, P., Buschelman, K., Constantinescu, E., Dalcin, L., Dener, A., Eijkhout, V., Gropp, W. D., Hapla, V., Isaac, T., Jolivet, P., Karpeev, D., Kaushik, D., Knepley, M. G., Kong, F., Kruger, S., May, D. A., McInnes, L. C., Mills, R. T., Mitchell, L., Munson, T., Roman, J. E., Rupp, K., Sanan, P., Sarich, J., Smith, B. F., Zampini, S., Zhang, H., Zhang, H., and Zhang, J., "PETSc/TAO Users Manual," Tech. Rep. ANL-21/39 Revision 3.16, Argonne National Laboratory, 2021.
- [16] Balay, S., Abhyankar, S., Adams, M. F., Benson, S., Brown, J., Brune, P., Buschelman, K., Constantinescu, E. M., Dalcin, L., Dener, A., Eijkhout, V., Gropp, W. D., Hapla, V., Isaac, T., Jolivet, P., Karpeev, D., Kaushik, D., Knepley, M. G., Kong, F., Kruger, S., May, D. A., McInnes, L. C., Mills, R. T., Mitchell, L., Munson, T., Roman, J. E., Rupp, K., Sanan, P., Sarich, J., Smith, B. F., Zampini, S., Zhang, H., Zhang, H., and Zhang, J., "PETSc Web page," https://petsc.org/, 2021. URL https://petsc.org/.
- [17] Anton Paar GmbH, "Viscosity of Paraffin Wax," Accessed 2023. URL https://wiki.anton-paar.com/en/paraffin-wax/.
- [18] Haj-Kacem, R., Ouerfelli, N., Herráez, J., Guettari, M., Hamda, H., and Dallel, M., "Contribution to modeling the viscosity Arrhenius-type equation for some solvents by statistical correlations analysis," *Fluid Phase Equilibria*, Vol. 383, 2014, pp. 11–20. https://doi.org/10.1016/j.fluid.2014.09.023.
- [19] Kobald, M., Toson, E., Ciezki, H., Schlechtriem, S., di Betta, S., Coppola, M., and DeLuca, L., "Rheological, optical, and ballistic investigations of paraffin-based fuels for hybrid rocket propulsion using a two-dimensional slab-burner," *Progress in Propulsion Physics*, Vol. 8, 2016, pp. 263–282. https://doi.org/https://doi.org/10.1051/eucass/201608263.
- [20] Piscitelli, F., Saccone, G., Gianvito, A., Cosentino, G., and Mazzola, L., "Microcrystalline paraffin wax as fuel for Hybrid Rocket Engine," 6TH EUROPEAN CONFERENCE FOR AERONAUTICS AND SPACE SCIENCES (EUCASS), 2015.
- [21] Karabeyoglu, M., Altman, D., and Bershader, D., "Transient combustion in hybrid rockets," *In 31st Joint Propulsion Conference and Exhibit*, Vol. 383, 1995, p. 2691. https://doi.org/https://doi.org/10.2514/6.1995-2691.
- [22] Fu, J., Hong, F., Wei, P., Guo, Z., Xu, Y., and Gao, W., "Combining Bayesian active learning and conditional Gaussian process simulation for propagating mixed uncertainties through expensive computer simulators," *Aerospace Science and Technology*, Vol. 139, 2023, p. 108363. https://doi.org/10.1016/j.ast.2023.108363.
- [23] Ignatyev, D. I., Shin, H.-S., and Tsourdos, A., "Sparse online Gaussian process adaptation for incremental backstepping flight control," *Aerospace Science and Technology*, Vol. 136, 2023, p. 108157. https://doi.org/https://doi.org/10.1016/j.ast.2023. 108157.
- [24] Yoshikawa, Y., and Iwata, T., "Gaussian Process Regression With Interpretable Sample-Wise Feature Weights," IEEE Transactions on Neural Networks and Learning Systems, Vol. 34, No. 9, 2023, pp. 5789–5803. https://doi.org/10.1109/TNNLS. 2021.3131234.
- [25] Rohmer, J., and Foerster, E., "Global sensitivity analysis of large-scale numerical landslide models based on Gaussian-Process meta-modeling," *Computers & Geosciences*, Vol. 37, No. 7, 2011, pp. 917–927. https://doi.org/https://doi.org/10.1016/j.cageo. 2011.02.020, URL https://www.sciencedirect.com/science/article/pii/S0098300411000951.
- [26] Palar, P. S., Parussini, L., Bregant, L., Shimoyama, K., and Zuhal, L. R., "On kernel functions for bi-fidelity Gaussian process regressions," *Structural and Multidisciplinary Optimization*, Vol. 66, No. 2, 2023, p. 37. https://doi.org/10.1007/s00158-023-03487-y.